

Nuclear Magnetic Relaxation Time near the Compensation Temperature in a Ferrimagnetic Insulator

Michiyasu Mori

Advanced Science Research Center, Japan Atomic Energy Agency, Tokai, Ibaraki 117-1195, Japan

The nuclear magnetic relaxation time T_1 in a ferrimagnetic insulators is calculated within the mean-field approximation for the magnetic exchange interactions and the Raman process involving the hyperfine interaction. We find that the value of $1/T_1$ on one type of site increases rapidly near the compensation temperature T_0 , whereas that on the other type of site does not increase up to Curie temperature T_c . This is due to the fact that the soft-magnon bandwidth becomes comparable to T_0 . An increase in $1/T_1$ below T_c is found also in another type ferrimagnet, which shows a hump structure in the temperature dependence of magnetization instead of compensation. Also in that case, we find the rapid increase in $1/T_1$ below T_c , even though the magnetization does not show compensation. The coexistence of soft and hard magnons leads to these remarkable properties of ferrimagnets.

1. Introduction

A *ferrimagnet* is a kind of *ferro-magnet*, and it was theoretically predicted by Néel.^{1–3)} Soon afterward, the magnetization compensation was observed in the LiFeCr spinel ferrite, for which the magnetization becomes zero at magnetization-compensation temperature T_M far below the Curie temperature T_c .⁴⁾ Such a ferrimagnet, called an N-type ferrimagnet, also has been found in rare-earth iron garnets (RIGs).^{2,5–11)} The RIGs have been studied by many authors in order to apply their magnetization-compensation properties to magneto-optical memories.^{12–14)}

The dynamical aspects of ferrimagnetism were initially studied using the electron spin resonance (ESR).^{15–23)} The ferrimagnetic resonance (FIR) differs from the ferromagnetic resonance (FMR) in having two branches. One gives the usual FMR, while the other, called the exchange frequency, is located higher in energy.²¹⁾ It was difficult to measure the exchange frequency when it was first discovered, since its wavelength is of the order of a tenth of a millimeter. However, a singular behavior of the gyromagnetic ratio was observed around the angular momentum compensation temperature T_A in a LiFeCr spinel ferrite.^{15,16)} On the lower branch, the effective gyromagnetic ratio becomes small around T_M and then increases rapidly around T_A .^{15–23)} The g -value of the upper branch becomes small in a measurable range around T_A .¹⁶⁾ The magnetization is the product of the Lande g -factor and a total angular momentum. In general, hence, T_M is different from T_A , when the orbital angular momentum is involved. In contrast to the magnetization, the dynamics of a ferrimagnet become singular around T_A .

Because the magnetization couples to a magnetic field, while the total angular momentum itself does not, it can be difficult to measure T_A directly using conventional methods. Recently, however, Imai et al. have successfully observed T_A using the Barnett effect.^{24–26)} In a rotating frame, the rotation frequency couples to the angular momentum instead of to the magnetization, without any coupling constant. By spin-rotation coupling, a magnetization is induced through the angular momentum by mechanical rotation. This was originally studied by Barnett,²⁷⁾ and it is now used to determine T_A in

a RIG.^{24,25)} It has been reported that around T_A the magnetization reverse rapidly and that domain walls move fast.^{28–31)} Those properties, which are advantageous for magnetic memories, are attributed to angular-momentum compensation.

Nuclear magnetic resonance (NMR) also is a powerful tool for studying the magnetism of a broad range of materials. Magnetic excitations can be characterized by the nuclear magnetic relaxation time T_1 , which originates in the hyperfine interaction between electron and nucleus. For magnetic insulators, however, the origin of T_1 is not so obvious. If the system is isotropic and the nuclear and electron quantization axes are identical, the relaxation cannot be obtained within the linearized spin-wave approximation. Misalignment of the quantization axes—and/or the dipole-dipole interactions between an electronic and a nuclear spins—induces relaxation through the Raman process.^{32–34)} Interactions among magnons are also the source of relaxation, e.g., through the three-magnon process.^{32–34)} Those processes can be studied for both ferromagnetic and antiferromagnetic insulators. Recently, Imai et al. have reported an enhancement of the NMR signal around T_A , which is closely related to domain wall motion.²⁶⁾ In contrast to ESR, NMR provides a site-selective measurement of magnetism. It is therefore interesting to study the dynamical aspects of magnetism site-by-site in a ferrimagnet. In addition, a consistent understanding of ferrimagnetism among experimental methods—NMR, ESR, and neutron scattering—will be useful.

In this paper, we study the nuclear magnetic relaxation time in ferrimagnets. Section 2 explains the model Hamiltonian and the approximation used. The nuclear magnetic relaxation time due to the Raman process is given in Sec. 3. Additional changes due to orbital angular momentum are briefly discussed in Sec. 4. Below, Bohr magneton μ_B and Planck constant $\hbar = h/2\pi$ are set equal to 1 for brevity.

2. Formalism: Magnons in Ferrimagnet

We will focus on a ferrimagnetic “insulator,” which is simply called a “ferrimagnet” below. The magnetic exchange interaction due to the Pauli principle and to the Coulomb interaction between electrons is the source of magnetism in a ferrimagnet. Two sub-lattices with different spin magnitudes

$S_A \neq S_B$ comprise the simplest model. The Hamiltonian is given by

$$H = -J_A \sum_{\langle i,i' \rangle} \vec{S}_i \cdot \vec{S}_{i'} - J_B \sum_{\langle j,j' \rangle} \vec{S}_j \cdot \vec{S}_{j'} + J_C \sum_{\langle i,j \rangle} \vec{S}_i \cdot \vec{S}_j, \quad (1)$$

with the spin operators \vec{S}_i (\vec{S}_j) on site $i \in A$ -sites ($j \in B$ -sites). The angular brackets $\langle \dots \rangle$ denotes nearest neighbor sites. The magnitudes of the magnetic exchange interactions J_A , J_B , and J_C are assumed to be positive for brevity. First, we do not consider the orbital angular momentum \vec{L}_i . Hence, there is only one compensation temperature T_0 ; i.e., $T_M = T_A \equiv T_0$. What is changed by \vec{L}_i will be discussed in the last section. At T_0 , the expectation values $\langle S_A^z \rangle \equiv M_A > 0$ and $\langle S_B^z \rangle \equiv -M_B < 0$ satisfy $M_A - M_B = 0$, where the bracket denotes the thermal average. See also Appendix A. It is known that there are some possible cases of compensation. In the case considered above, both sub-lattices have the same number of sites in a unit cell, as shown in the inset of Fig. 1. Another case has $M_A n_A - M_B n_B = 0$, for which the number n_A of spins on sub-lattice A is different from the number n_B on sub-lattice B. As shown in Appendix B, those lattice structures have characteristic features in common. Hence, we consider the simplest case, shown in Fig. 1 below.

Compensation occurs at a finite temperature. To include the temperature dependences of M_A and M_B , we adopt the mean-field approximation and use the linearized spin-wave approximation around the mean-field solution. This is equivalent to Tyablikov decoupling in the Green's function method and is a kind of random-phase approximation.^{35,36} The mean-field solution for $J_A=0.1$, $J_B=1.0$, $J_C=0.05$, $S_A=1$, and $S_B=1/2$, is shown in Fig. 1, where $T_0/T_c \sim 0.3$ and the Curie temperature is $T_c \sim 3.0$.

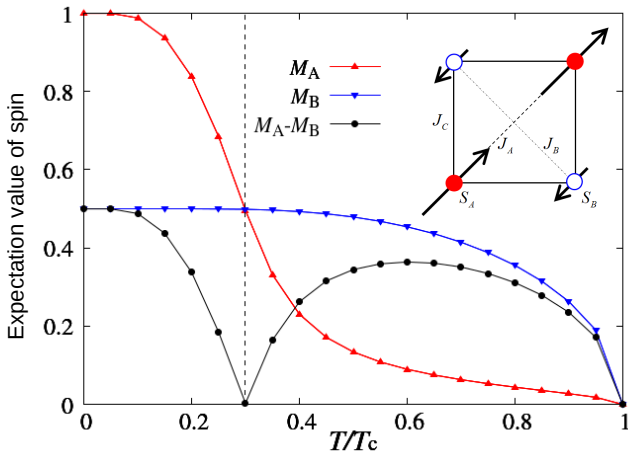


Fig. 1. (Color online) The mean-field solution for $J_A=0.1$, $J_B=1.0$, $J_C=0.05$, $S_A=1$, and $S_B=1/2$. The inset shows the lattice structure, which is three dimensional. The red (upward) and blue (downward) triangles denote M_A and M_B , respectively. The black circles are the sum of two expectation values, $M_A - M_B$. The broken line indicates T_0 .

The Holstein-Primakoff (HP) bosons (magnons)—for which the creation and annihilation operators are a_i^\dagger, a_i on A-sublattice and b_j^\dagger, b_j on B-sublattice—are given by, $S_i^- \sim \sqrt{2M_A}a_i^\dagger$, $S_i^+ \sim \sqrt{2M_A}a_i$, $S_i^z = M_A - a_i^\dagger a_i$, $S_j^- \sim \sqrt{2M_B}b_j^\dagger$, $S_j^+ \sim \sqrt{2M_B}b_j$, $S_j^z = M_B - b_j^\dagger b_j$. Below, the spins are assumed to be ordered in the z -direction. By the linearized approximation, the action of the magnons is given by³⁷⁾

$$S = \sum_{q, i\omega_n} \Phi^\dagger \left[\begin{pmatrix} -i\omega_n & 0 \\ 0 & i\omega_n \end{pmatrix} + \begin{pmatrix} \varepsilon_{1q} & \varepsilon_{3q}^* \\ \varepsilon_{3q} & \varepsilon_{2q} \end{pmatrix} \right] \Phi, \quad (2)$$

$$\Phi^\dagger \equiv (a_q^\dagger(i\omega_n), b_{-q}(-i\omega_n)), \quad (3)$$

$$\varepsilon_{1q} \equiv zJ_C M_B + z_A J_A M_A (1 - \zeta_{Aq}), \quad (4)$$

$$\varepsilon_{2q} \equiv zJ_C M_A + z_B J_B M_B (1 - \zeta_{Bq}), \quad (5)$$

$$\varepsilon_{3q} \equiv J_C \sqrt{M_A M_B} \sum_{\xi} e^{iq \cdot \xi}, \quad (6)$$

$$\zeta_{A(B)q} \equiv \frac{1}{z_{A(B)}} \sum_{\eta} \cos(\mathbf{q} \cdot \boldsymbol{\eta}), \quad (7)$$

We use the boson operators $a_q(i\omega_n)$ and $b_{-q}(-i\omega_n)$ with momentum $\mathbf{q}=(q_x, q_y, q_z)$ and Matsubara frequency ω_n . The \mathbf{q} -summation is taken over the first Brillouin zone. The magnon dispersion relation depends on the connectivity of the sub-lattice, which gives the number of nearest-neighbor sites z_A and z_B on each sub-lattice, and the number z of nearest-neighbor sites between the two sub-lattices. In Eqs. (6) and (7), ξ and η mean the summation over the nearest-neighbor sites between the two sub-lattices and within each sublattice, respectively. From Eq. (2), the magnon Green's functions $g_\nu(\mathbf{q}, i\omega_n)$ are given by

$$\begin{aligned} g_A(\mathbf{q}, i\omega_n) &\equiv \langle a_q(i\omega_n) a_q^\dagger(i\omega_n) \rangle \\ &= -\frac{i\omega_n + \varepsilon_{2q}}{(i\omega_n - E_{\alpha q})(i\omega_n + E_{\beta q})}, \end{aligned} \quad (8)$$

$$\begin{aligned} g_B(\mathbf{q}, i\omega_n) &\equiv \langle b_q(i\omega_n) b_q^\dagger(i\omega_n) \rangle \\ &= -\frac{i\omega_n + \varepsilon_{1q}}{(i\omega_n - E_{\beta q})(i\omega_n + E_{\alpha q})}, \end{aligned} \quad (9)$$

and the magnon dispersion relations $E_{\alpha q}$ and $E_{\beta q}$ are given by

$$E_{\alpha q} = \frac{1}{2} \left[(\varepsilon_{1q} - \varepsilon_{2q}) + \sqrt{(\varepsilon_{1q} + \varepsilon_{2q})^2 - 4|\varepsilon_{3,q}|^2} \right], \quad (10)$$

$$E_{\beta q} = \frac{1}{2} \left[-(\varepsilon_{1q} - \varepsilon_{2q}) + \sqrt{(\varepsilon_{1q} + \varepsilon_{2q})^2 - 4|\varepsilon_{3,q}|^2} \right]. \quad (11)$$

The small- Q approximation for $M_A > M_B$ leads to,

$$E_{\alpha q} \sim CQ^2, \quad (12)$$

$$E_{\beta q} \sim 12J_C (M_A - M_B) + DQ^2, \quad (13)$$

where C and D are constants given in Appendix B and $Q \equiv \sqrt{q_x^2 + q_y^2 + q_z^2}$. The mode $E_{\alpha q}$ is gapless, while $E_{\beta q}$ has an "optical gap," $E_g \equiv |E_{\alpha q=0} - E_{\beta q=0}| = 12J_C (M_A - M_B)$, which disappears at T_0 . The dispersion relations degenerate at the gamma point and increases linearly with Q , similar to an anti-ferromagnet. Away from the gamma point, on the other hand, the two dispersion relations deviate from each other:

$$E_{\alpha q} \sim C_1 Q + C_2 Q^2, \quad (14)$$

$$E_{\beta q} \sim C_1 Q - C_2 Q^2, \quad (15)$$

where C_1 and C_2 are constants given in Appendix B. These Q -dependences are relevant to the temperature dependence of T_1 at low temperatures.

3. Results: Nuclear Magnetic Relaxation due to the Raman Process

In this study, we consider the nuclear magnetic relaxation time T_1 originating from the contact interaction between a nucleus and an electron

$$H_{n-el} = \frac{1}{2} \sum_{\nu=A,B} \left[\gamma_\nu \sum_i f_{i\nu} (\vec{S}_i \cdot \vec{I}_i) \right], \quad (16)$$

with the g -factor on ν -sites being given by γ_ν and the nuclear spin \vec{I}_i on i -site. If the system is isotropic and the quantization axes of the nucleus and electron are identical, we cannot obtain relaxation within the linearized approximation. Misalignment of the quantization axes—and/or the dipole-dipole interactions between electronic and nuclear spins—will induce relaxation due to the Raman process.^{32–34} Interactions among magnons also cause relaxation, e.g., through the three magnon-process.^{32–34} Below, we focus on the Raman process induced by misalignment. This is sufficient to enable us to find some of the characteristics of T_1 near T_0 . The critical exponent of T_1 is beyond the scope of this study and will be discussed elsewhere. When the quantization axis of nucleus deviates by an angle θ from that of the electron, Eq. (16) reduces to the following component

$$H_{n-el}^z = \frac{1}{2} \sum_{\nu=A,B} \left[\gamma_\nu \sum_i \sin \theta f_{i\nu} S_i^z (I_i^+ + I_i^-) \right], \quad (17)$$

which are relevant for calculating T_1 . Assuming that $\gamma_A = \gamma_B \equiv \gamma$ and the form factors f_{iA} are constant, i.e., $f_{iA} = f_{iB} \equiv f$, the T_1 on site $\nu = A, B$ is given by

$$\frac{1}{T_{1\nu}} = F \sum_{\mathbf{q}} C_\nu(\mathbf{q}, \omega_0), \quad (18)$$

$$C_\nu(\mathbf{q}, \omega_0) = \int dt e^{i\omega_0 t} \langle S_{\nu\mathbf{q}}^z(t) S_{\nu-\mathbf{q}}^z(0) + S_{\nu-\mathbf{q}}^z(t) S_{\nu\mathbf{q}}^z(0) \rangle, \quad (19)$$

where $\langle \cdots \rangle$ means the thermal average. The nuclear magnetic resonance energy is denoted by ω_0 , and $F = (\gamma f \sin \theta / 2)^2$. Using Eqs. (8) and (9), the spin-spin correlation function $C_\nu(\mathbf{q}, \omega_0)$ is given by

$$C_\nu(\mathbf{q}, \omega_0) = \frac{2}{1 - e^{\omega_0/k_B T}} \text{Im} \Pi_\nu^R(\mathbf{q}, \omega_0), \quad (20)$$

$$\Pi_\nu(\mathbf{q}, i\omega_0) = k_B T \sum_{\mathbf{p}, n} g_\nu(\mathbf{p} + \mathbf{q}, i\omega_n + i\omega_0) g_\nu(\mathbf{p}, i\omega_n), \quad (21)$$

where T is temperature, k_B is the Boltzmann's constant, and momentum $\mathbf{p} = (p_x, p_y, p_z)$ in the first Brillouin zone. The retarded function of $\Pi_\nu(\mathbf{q}, i\omega_0)$ is denoted by $\Pi_\nu^R(\mathbf{q}, \omega_0)$. When ω_0 is much smaller than $k_B T$, the nuclear magnetic relaxation time $T_{1\nu}$ on site ν is given by

$$\begin{aligned} \frac{1}{T_{1\nu}} &= 2F \sum_{\mathbf{q}} \lim_{\omega_0 \rightarrow 0} \frac{k_B T}{\omega_0} \text{Im} \Pi_\nu^R(\mathbf{q}, \omega_0), \\ &= 2\pi F \sum_{\mathbf{p}, \mathbf{q}} \left\{ n_B(E_{\nu\mathbf{p}}) [n_B(E_{\nu\mathbf{p}}) + 1] \frac{\alpha_{\mathbf{p}} \alpha_{\mathbf{q}}}{\Delta_{\mathbf{p}} \Delta_{\mathbf{q}}} \delta(E_{\nu\mathbf{p}} - E_{\nu\mathbf{q}}) \right. \end{aligned} \quad (22)$$

$$\left. + n_B(E_{\mu\mathbf{p}}) [n_B(E_{\mu\mathbf{p}}) + 1] \frac{\beta_{\mathbf{p}} \beta_{\mathbf{q}}}{\Delta_{\mathbf{p}} \Delta_{\mathbf{q}}} \delta(E_{\mu\mathbf{p}} - E_{\mu\mathbf{q}}) \right\}, \quad (23)$$

$$\frac{\alpha_{\mathbf{p}}}{\Delta_{\mathbf{p}}} = \frac{1}{2} \left(\frac{\varepsilon_{1\mathbf{p}} + \varepsilon_{2\mathbf{p}}}{\Delta_{\mathbf{p}}} + 1 \right), \quad (24)$$

$$\frac{\beta_{\mathbf{p}}}{\Delta_{\mathbf{p}}} = \frac{1}{2} \left(\frac{\varepsilon_{1\mathbf{p}} + \varepsilon_{2\mathbf{p}}}{\Delta_{\mathbf{p}}} - 1 \right), \quad (25)$$

$$\Delta_{\mathbf{p}} = \sqrt{(\varepsilon_{1\mathbf{p}} + \varepsilon_{2\mathbf{p}})^2 - 4|\varepsilon_{3\mathbf{p}}|^2}, \quad (26)$$

Here $\mu \neq \nu$, i.e., $\mu=\alpha$ for $\nu=\beta$ or $\mu=\beta$ for $\nu=\alpha$ and the Bose distribution function is denoted by $n_B(x) \equiv 1/[e^{x/(k_B T)} - 1]$. Note that Eq. (23) can be checked by considering the ferro- and the antiferromagnet cases as discussed in Appendix C.

Using Eq. (23) and the mean-field solution shown in Fig. 1, the T -dependence of $1/T_{1\nu}$ can be calculated numerically as shown in Fig. 2 (a). Note that $1/T_{1A}$ increases rapidly around

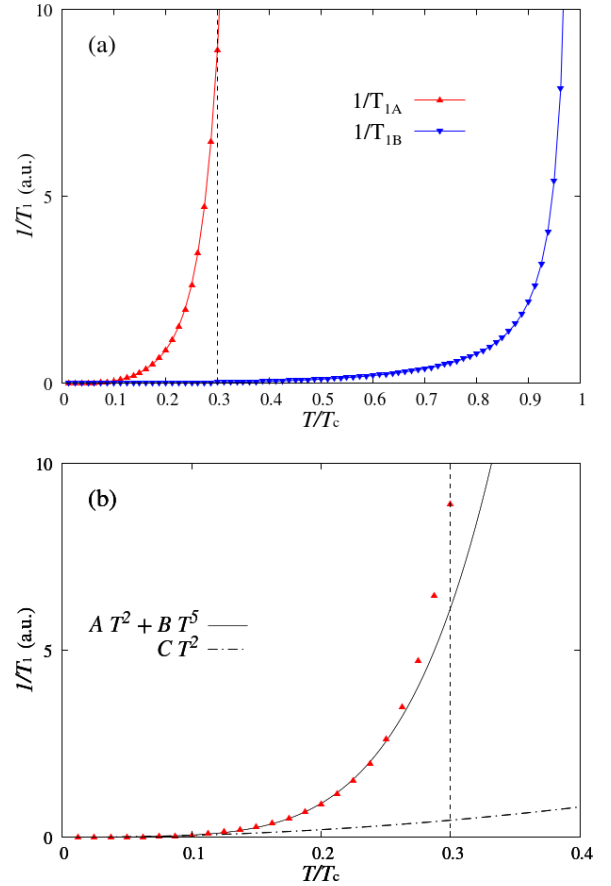


Fig. 2. (Color online) (a) The T -dependence of $1/T_1$ on the A-sites and B-sites ($1/T_{1A}$ and $1/T_{1B}$) are plotted with upward triangles (red) and downward triangles (blue), respectively. The mean-field solution for $J_A=0.1$, $J_B=1.0$, $J_C=0.05$, $S_A=1$, and $S_B=1/2$ was used. The broken line indicates T_0 . See also Fig. 1. (b) At low temperatures, T_{1A} is well fitted by T^2 (the dashed-dotted line) similar to the ferromagnet (See also Appendix C), whereas it is deviated with increasing temperature as $AT^2 + BT^5$ (solid line). A and B are constants.

$T/T_c \sim 0.3$, which corresponds to T_0 indicated by the broken line in Fig. 2. This contrasts sharply with $1/T_{1B}$, which diverges just below T_c . As shown in Fig. 2 (b), at low temperatures, T_{1A} is well fitted by T^2 , similar to the ferromagnet

(See also Appendix C). With increasing temperature, on the other hand, it is fitted by $AT^2 + BT^5$ with constants A and B . This is similar to the behavior of a ferromagnet, except for the fact that $1/T_{1A}$ increases around T_0 instead of T_c .

To understand this behavior of $1/T_1$ around T_0 , $E_{\alpha q}$ and $E_{\beta q}$ are plotted in Fig. 3 for (a) $T/T_c = 0.1$ and (b) $T/T_c = 0.3$ with $q_y = q_z = 0$. At low temperatures, the T -dependence of $1/T_1$

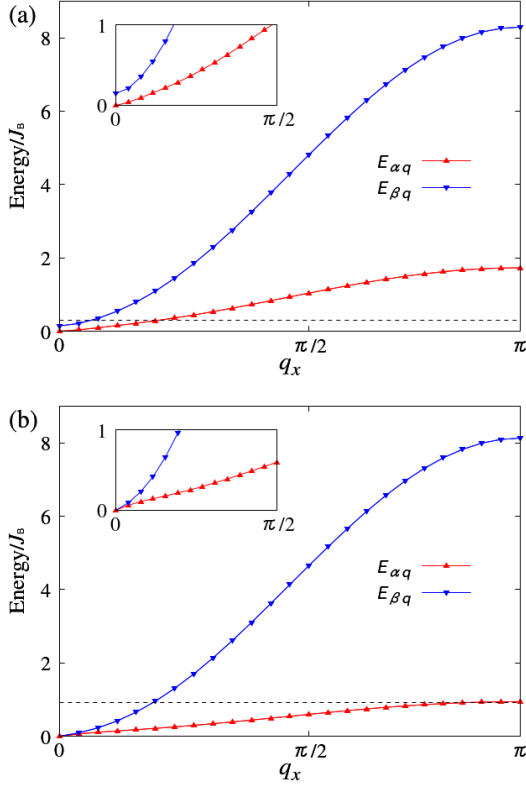


Fig. 3. (Color online) The dispersion relations $E_{\alpha q}$ and $E_{\beta q}$ are plotted by upward triangles (red) and downward triangles (blue), respectively, for (a) $T/T_c = 0.1$ and (b) $T/T_c = 0.3$, with $q_y = q_z = 0$. In the pre-set lattice structure, at $\mathbf{q} = (\pi, \pi/2, 0)$, $E_{\alpha q}$ is a maximum. This can be approximated by its value at $\mathbf{q} = (\pi, 0, 0)$ due to the small value of J_C . The low-energy region is enlarged and plotted in the insets.

is determined by the Q^2 -dependences of $E_{\alpha q}$ and $E_{\beta q}$ around $Q \sim 0$. See also the inset of Fig. 3 (a). At $T = T_0$, E_g becomes zero, as shown in the inset of Fig. 3 (b), and both $E_{\alpha q}$ and $E_{\beta q}$ become proportional to Q instead of Q^2 around $Q = 0$. Note that $k_B T/J_B$ is shown by the broken line in Figs. 3 (a) and (b) as a measure of the temperature. In the pre-set lattice structure, $E_{\alpha q}$ is a maximum at $\mathbf{q} = (\pi, \pi/2, 0)$. It can be approximated by the value at $\mathbf{q} = (\pi, 0, 0)$, since the small value of $J_C = 0.05$. We then find that at $T = T_0$ the bandwidth of $E_{\alpha q}$ becomes comparable to $k_B T$. This means that all states of $E_{\alpha q}$ contribute to $1/T_1$ through $n_B(x)$ in the first term in Eq. (23), where the first term is dominant. This is the origin of the rapid increase in $1/T_{1A}$ at T_0 . This is not accidental, due to the following points. The bandwidth of $E_{\alpha q}$ can be very roughly estimated by $\varepsilon_{1, \mathbf{q}=(\pi, 0, 0)} \sim (6J_C + 16J_A)M_0 \sim 8J_A = 0.8$ with $M_A = M_B \equiv M_0 \sim 0.5$. On the other hand, T_0 can be roughly estimated as $T_0 \sim z_A J_A X_A = 0.8$. Since M_A is soft and decreases rapidly with T , T_0 is close to the Curie temperature of a system limited to the A -sublattice. Therefore, $1/T_{1A}$

rapidly increases around T_0 .

So far, we have discussed an N -type ferrimagnet.^{1,3)} Another type of ferrimagnet—called P -type—shows a hump in the temperature dependence of the magnetization instead of compensation. Figure 4 is calculated from Eq. (1) for $J_A=0.5$, $J_B=1.0$, $J_C=0.2$, $S_A=1/2$, and $S_B=1$. The lattice structure is the same as the inset of Fig. 1. In a P -type ferrimagnet, the

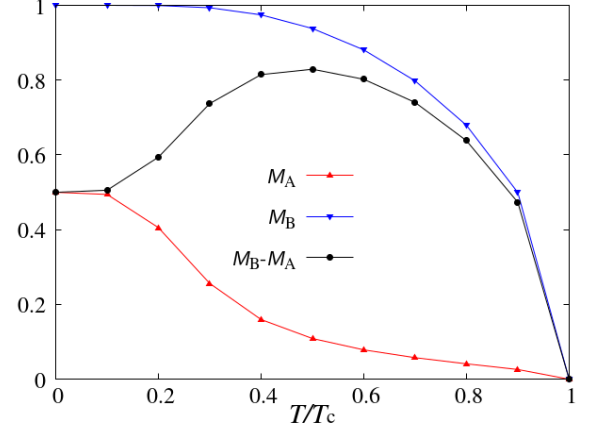


Fig. 4. (Color online) The mean-field solution for a P -type ferrimagnet with $J_A=0.5$, $J_B=1.0$, $J_C=0.2$, $S_A=1/2$, and $S_B=1$.

magnetization does not show any singular behavior, such as compensation, although it is composed of two different sublattices, i.e., with soft and hard dispersion relations $E_{\alpha q}$ and $E_{\beta q}$. The value of $1/T_{1v}$ in a P -type ferrimagnet is plotted in Fig. 5 in the same way as for the N -type. We find that $1/T_{1A}$

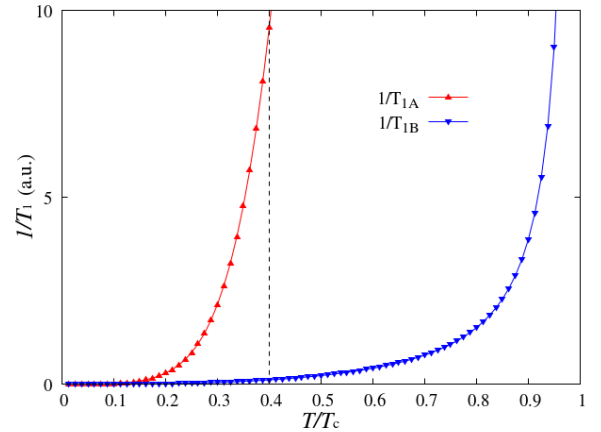


Fig. 5. (Color online) The relaxation rate $1/T_1$ in a P -type ferrimagnet. The T -dependences of $1/T_1$ on the A -sites and B -sites ($1/T_{1A}$ and $1/T_{1B}$) are plotted by upward triangles (red) and downward triangles (blue), respectively. The mean-field solution for $J_A=0.5$, $J_B=1.0$, $J_C=0.2$, $S_A=1/2$, and $S_B=1$ was used. The broken line is near the top of the hump structure.

rapidly increases around $T/T_c \sim 0.4$ close to the top of the hump structure, while $1/T_{1B}$ increases rapidly near T_c . It is now straightforward to understand this behavior, since the A -sublattice is soft and the B -sublattice is hard. This is clearly shown by the dispersion relation in Figs. 6 for (a) $T/T_c = 0.1$

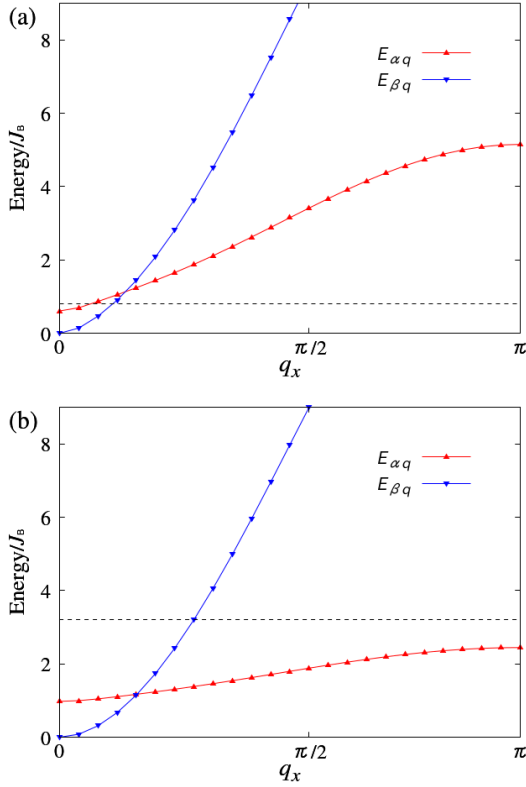


Fig. 6. (Color online) The dispersion relations $E_{\alpha q}$ and $E_{\beta q}$ are plotted by upward triangles (red) and downward triangles (blue), respectively, for (a) $T/T_c = 0.1$ and (b) $T/T_c = 0.4$, with $q_y = q_z = 0$. The broken line indicates the corresponding temperature $k_B T/J_B$.

and (b) $T/T_c = 0.4$. In each panel, $k_B T/J_B$ is shown by the broken line as measure of the temperature. At $T/T_c = 0.4$, all of $E_{\alpha q}$ contribute to $1/T_{1A}$. Therefore, even in a P -type ferrimagnet without compensation, we find a rapid increase of $1/T_1$.

4. Summary and Discussions

We have studied T_1 in a ferrimagnetic insulator that is induced by the Raman process involving the hyperfine interaction. To calculate $1/T_1$, we adopted a Heisenberg model composed of two sublattices and used the linearized spin-wave approximation around the mean-field solution. At $T_0 < T_c$, $1/T_1$ increases rapidly on one sublattice, whereas on the other site it does not increase up to T_c , as usual in a ferromagnet. This is due to the fact that an N -type ferrimagnet has two magnon excitations. The soft magnon contributes to the increasing behavior of $1/T_1$ at T_0 , since the bandwidth of the soft magnon is less than T_0 in energy.

At low temperatures, the T -dependence of $1/T_1$ is well fitted by T^2 , similar to the ferromagnetic case. With increasing temperature, a T^5 -component is added, due to the momentum dependence of the dispersion relation. In this paper, however, we have considered only the Raman process. When the three-magnon process, magnon-magnon interactions, and other factors are involved, those T -dependences will be modified. Those are beyond the purpose of this paper and will be studied elsewhere.

The increase in $1/T_1$ below T_c is found also in a P -type ferrimagnet, which shows hump structure in the temperature de-

pendence of the magnetization instead of compensation. Also in a P -type ferrimagnet, we find a rapid increase of $1/T_1$ below T_c , even though the magnetization does not show compensation. This also can be explained by the fact that a P -type ferrimagnet is composed of soft and hard magnons. Although a P -type ferrimagnet does not show compensation, $1/T_1$ on one sublattice still increases below T_c . We expect this to be experimentally confirmed in the near future.

So far, we have not considered the orbital angular momentum \vec{L} . For example, in rare-earth (R) iron garnets, $R_3\text{Fe}_5\text{O}_{12}$ ($R=\text{Ho, Er, Tb, etc.}$), the rare-earth magnetization is calculated by using the total angular momentum $\vec{J} = \vec{L} + \vec{S}$.³⁸⁾ The Landé g -factor on an R-site is different from that on an iron site, and $T_M \neq T_A$ in general. Still, Eq. (1) is our starting point. The expectation value of S_A^z then contains the extra factor $(\gamma_A - 1)$, so that $\langle S_A^z \rangle = (\gamma_A - 1) \langle J_A^z \rangle$,³⁸⁾ where J_v^z is the z -component of \vec{J} on v -site ($v=A, B$). These factors can be renormalized into J_A , J_B , and J_C : $K_A \equiv (\gamma_A - 1)^2 J_A$, $K_B \equiv (\gamma_B - 1)^2 J_B$, and $K_C \equiv (\gamma_A - 1)(\gamma_B - 1) J_C$.^{39,40)} Using K_A , K_B , and K_C , the magnon dispersion relations are obtained by substituting $\langle J_A^z \rangle$ and $\langle J_B^z \rangle$ for M_A and M_B , respectively. See also Appendix D. Around which temperature, T_M or T_A , does $1/T_1$ start to increase? The magnon bandwidth is determined by the expectation value of $\langle S_A^z \rangle = (\gamma_A - 1) \langle J_A^z \rangle$ and $\langle S_B^z \rangle = (\gamma_B - 1) \langle J_B^z \rangle$ instead of $\langle J_A^z \rangle$ and $\langle J_B^z \rangle$. We recall that $1/T_1$ increases, when $k_B T$ is comparable to the bandwidth, and T_A is determined by $\langle J_A^z \rangle$ and $\langle J_B^z \rangle$. For example, in a case with $\gamma_A = 5/4$, $\gamma_B = 2$, such as for $\text{Ho}_3\text{Fe}_5\text{O}_{12}$, the factors $(\gamma_A - 1)$ and $(\gamma_B - 1)$ are smaller than 1. A rough estimate of the energy scale of the bandwidth is thus smaller than T_A . This means that $1/T_1$ will start to increase further below T_A . However, those energy scales are different depending on the materials involved. Thus, it is difficult to identify the temperature at which $1/T_1$ starts to increase. Such a material dependence will be discussed in the near future and will be clarified experimentally.

On the other hand, it is clear that E_g becomes zero at T_A instead of T_M

$$E_g = 12K_C [\langle J_A^z \rangle - \langle J_B^z \rangle]. \quad (27)$$

Magnon excitations in RIGs have been reported from inelastic neutron scattering.^{41,42)} However, E_g has not yet been clarified around the compensation temperature. The loss of E_g must be associated with the increase of domain wall speed at T_A ^{28–31)} and the enhancement of NMR signals.²⁶⁾ Such remarkable changes of the domain walls will make ferrimagnets more useful for spintronics. A consistent understanding of the NMR, ESR, and neutron-scattering results will be even more important and useful.

The author thanks S. Maekawa, H. Chudo, M. Imai, M. Fujita, Y. Kawamoto, S. Kambe, Y. Tokunaga, and H. Sakai for useful and helpful discussions. This work was supported by Grants-in-Aid for Scientific Research (Grant 18H04492 and 20K03810) from JSPS and MEXT, and by the inter-university cooperative research program of IMR Tohoku University (20N0006). A part of the numerical calculation was done with the supercomputer of JAEA.

Appendix A: Mean-field Equation

The mean-field equation and its solution are straightforward. We define

$$M_A = f_{S_A} [(z_A J_A M_A - z_J J_C M_B) / (k_B T)], \quad (\text{A}\cdot 1)$$

$$M_B = f_{S_B} [(z_B J_B M_B - z_J J_C M_A) / (k_B T)], \quad (\text{A}\cdot 2)$$

$$f_S[x] \equiv (S + 1/2) \coth [x(S + 1/2)] - 1/2 \coth (x/2). \quad (\text{A}\cdot 3)$$

Note that g and μ_B have been omitted to make the equations clearer. Solving Eqs. (A·1) and (A·2) gives T_c in the form

$$T_c = \frac{1}{2} \left[X_A z_A J_A + X_B z_B J_B + \sqrt{(X_A z_A J_A - X_B z_B J_B)^2 + X_A X_B (2z_J J_C)^2} \right], \quad (\text{A}\cdot 4)$$

$$X_A \equiv (S_A + 1)S_A/3, \quad (\text{A}\cdot 5)$$

$$X_B \equiv (S_B + 1)S_B/3, \quad (\text{A}\cdot 6)$$

For the case shown in Fig. 1, T_0 can be approximated by the Curie temperature of the system limited to the A -sublattice, it is given by $T_0 \sim z_A J_A X_A$.

Appendix B: Magnon Dispersion Relations in a Ferri-magnet

At low energies away from the compensation temperature, the magnon dispersion relations given by Eqs. (10) and (11) can be expanded as

$$E_{\alpha q} \sim C Q^2, \quad (\text{B}\cdot 1)$$

$$E_{\beta q} \sim 12J_C (M_A - M_B) + D Q^2, \quad (\text{B}\cdot 2)$$

$$C = \frac{[3J_A M_A^2 - (J_A + J_B - 2J_C) M_A M_B + 3J_B M_B^2]}{M_A - M_B}, \quad (\text{B}\cdot 3)$$

$$D = \frac{J_A M_A^2 - (3J_A + 3J_B + 2J_C) M_A M_B + J_B M_B^2}{M_A - M_B}, \quad (\text{B}\cdot 4)$$

$$\varepsilon_{1q} + \varepsilon_{2q} = 6J_C (M_A + M_B) + 4(J_A M_A + J_B M_B) Q^2, \quad (\text{B}\cdot 5)$$

$$\Delta_q = 6J_C (M_A - M_B) + \frac{12J_C (M_B + M_A) (J_A M_A + J_B M_B) + 24J_C^2 M_A M_B}{6J_C (M_A - M_B)} Q^2, \quad (\text{B}\cdot 6)$$

where $Q \equiv \sqrt{q_x^2 + q_y^2 + q_z^2}$. Note that $(0,0,0)$ and (π, π, π) are equivalent for the case shown in Fig. 1. At the compensation temperature $M_A = M_B \equiv M$, the excitation gap vanishes

$$E_{\alpha q} \sim C_2 Q^2 + C_1 Q, \quad (\text{B}\cdot 7)$$

$$E_{\beta q} \sim -C_2 Q^2 + C_1 Q, \quad (\text{B}\cdot 8)$$

$$C_1 = 2\sqrt{3}J_C (J_A + J_B + J_C) S, \quad (\text{B}\cdot 9)$$

$$C_2 = 2(J_A - J_B) S, \quad (\text{B}\cdot 10)$$

$$\varepsilon_{1q} + \varepsilon_{2q} = 12J_C S + 4(J_A + J_B) S Q^2, \quad (\text{B}\cdot 11)$$

$$\Delta_q = 4S \sqrt{3J_C (J_A + J_B + J_C)} Q. \quad (\text{B}\cdot 12)$$

This does not depend on the lattice structure, as shown in Fig. B·1.

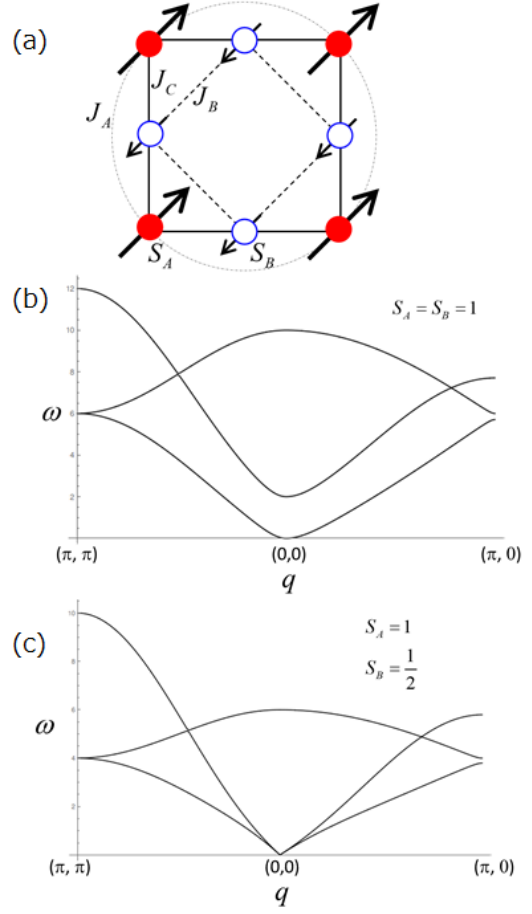


Fig. B-1. (Color online) (a) Schematic illustration of the compensation. The A -sublattice has one site, whereas the B -sublattice two sites. (b) Magnon dispersion relation away from the compensation point for $J_A=J_B=J_C=1$, $S_A=S_B=1$. (c) Magnon dispersion relation at the compensation point for $J_A=J_B=J_C=1$, $S_A=1$ and $S_B=1/2$. In both (b) and (c), the parameters were chosen by hand to show the characteristics.

Appendix C: Nuclear Magnetic Relaxation in a Ferromagnet and an Antiferromagnet

The ferromagnetic state is obtained by imposing the conditions $S_B=0$ and $J_C=J_B=0$ on the mean-field equation given by Eq. (1). Equation (23) then reduces to

$$\frac{1}{T_1} = 2\pi F \sum_{p,q} n_B(E_p) [n_B(E_p) + 1] \times \delta(E_p - E_q), \quad (\text{C}\cdot 1)$$

with $E_q = z_A J_A M_A (1 - \zeta_{Aq})$. The temperature dependence of $1/T_1$ is shown in Fig. C·1. At low temperatures, it is well fitted by CT^2 , because $E_q \propto Q^2$.^{33,34)} On the other hand, it deviates from T^2 with increasing T and is well fitted by $AT^2 + BT^5$, since a Q -linear component grows in E_q . Here, A , B , and C are constants.

The antiferromagnetic state is given by $S_A = S_B$ and $J_A = J_B = 0$. In this case, $E_{\alpha q} = E_{\beta q}$. Equation (23) then reduces to

$$\frac{1}{T_{1,v}} = 2\pi A_v \sum_{p,q} n_B(E_{vp}) [n_B(E_{vp}) + 1] \left[\frac{\varepsilon_p \varepsilon_q}{\Delta_p \Delta_q} + \frac{1}{4} \right]$$

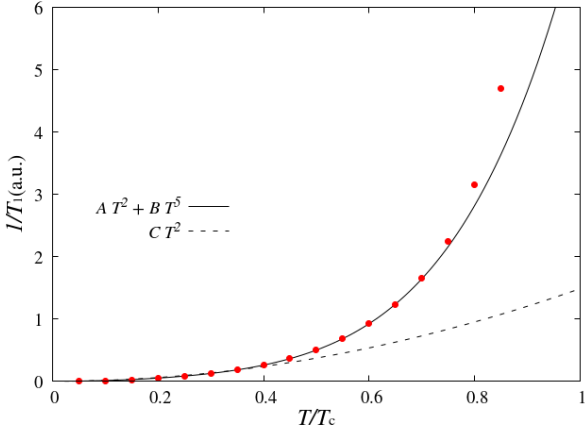


Fig. C-1. (Color online) The T -dependence of $1/T_1$ in the ferromagnetic state. The red dots were calculated numerically from Eq. (C-1) and the mean-field solution. The thick and the broken lines are fitting results using $AT^2 + BT^5$ and CT^2 , respectively.

$$\times \delta(E_{vp} - E_{vq}), \quad (\text{C-2})$$

where $\Delta_p = 2\sqrt{\varepsilon_p^2 - |\varepsilon_{3,p}|^2}$ and $\varepsilon_p = \varepsilon_{1p} = \varepsilon_{2p}$. Its temperature dependence is shown in Fig. C-2. At low temperatures, it is

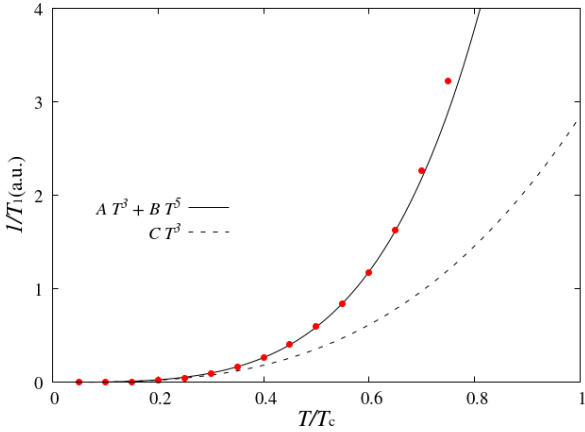


Fig. C-2. (Color online) The T -dependence of $1/T_1$ in the antiferromagnetic state. The red dots were calculated numerically from Eq. (C-2) and the mean-field solution. The thick and the broken lines are fitting results using $AT^3 + BT^5$ and CT^3 , respectively.

well fitted by CT^3 , because $E_q \propto Q$ and $(\varepsilon_q/\Delta_q) \propto Q^{-1}$.^{32,34} On the other hand, it deviates from T^3 with increasing T and is well fitted by $AT^3 + BT^5$, since the curvature of E_q becomes relevant. Here, A , B , and C are constants.

Appendix D: ESR Frequencies

When we consider \vec{L} , J_A , J_B , and J_C are replaced by K_A , K_B , and K_C , and further M_A and $-M_B$ are interpreted as $\langle J_A^z \rangle$ and $-\langle J_B^z \rangle$ in Eqs. (10) and (11). In a magnetic field $\vec{H} = (0, 0, H)$, $\gamma_A H$ and $-\gamma_B H$ are added to Eqs. (4) and (5), respectively. The magnon excitations at $Q = 0$, which correspond to the

ESR frequencies Ω_α and Ω_β are given by

$$\Omega_\alpha = \frac{1}{2} \left[(\varepsilon_1 - \varepsilon_2) + \sqrt{(\varepsilon_1 + \varepsilon_2)^2 - 4|\varepsilon_3|^2} \right], \quad (\text{D-1})$$

$$\Omega_\beta = \frac{1}{2} \left[-(\varepsilon_1 - \varepsilon_2) + \sqrt{(\varepsilon_1 + \varepsilon_2)^2 - 4|\varepsilon_3|^2} \right]. \quad (\text{D-2})$$

$$\varepsilon_1 = \lambda \langle J_B^z \rangle + \gamma_A H, \quad (\text{D-3})$$

$$\varepsilon_2 = \lambda \langle J_A^z \rangle - \gamma_B H, \quad (\text{D-4})$$

$$\varepsilon_3 = \lambda \sqrt{\langle J_A^z \rangle \langle J_B^z \rangle}, \quad (\text{D-5})$$

with $\lambda = zK_C$. At low temperatures—below both T_M and T_A —and to first order in H , Eqs. (D-1) and (D-2) for $\langle J_A^z \rangle - \langle J_B^z \rangle > 0$ can be approximated as^{17–23}

$$\Omega_\alpha \sim \frac{\gamma_A \langle J_A^z \rangle - \gamma_B \langle J_B^z \rangle}{\langle J_A^z \rangle - \langle J_B^z \rangle} H \equiv \gamma_{\text{eff}} H, \quad (\text{D-6})$$

$$\Omega_\beta \sim \lambda (\langle J_A^z \rangle - \langle J_B^z \rangle) - \frac{\gamma_B \langle J_A^z \rangle - \gamma_A \langle J_B^z \rangle}{\langle J_A^z \rangle - \langle J_B^z \rangle} H, \quad (\text{D-7})$$

with the effective gyromagnetic ratio γ_{eff} . At T_A , note that the two frequencies become close each other, since $\Omega_\alpha - \Omega_\beta = (\gamma_A + \gamma_B)H$.

- 1) L. Néel, Ann. Phys. (Paris) **12** 137 (1948).
- 2) L. Néel, R. Pauthenet, and B. Dreyfus, in *Progress Low Temperature Physics* ed. C.J. Gorter (North Holland, Amsterdam 1964) vol. 4 Chap. VII, p.344.
- 3) L. Néel, Science **174**, 985 (1971).
- 4) E. W. Gorter and J. A. Schulkes, Phys. Rev. **90**, 487 (1953).
- 5) R. Pauthenet and P. Blum, Compt. Rend. **239**, 33 (1954).
- 6) F. Bertaut and F. Forrat Compt. Rend. **242**, 382 (1956).
- 7) S. Geller and M. A. Gilleo, Acta Cryst. **10**, 239 (1957).
- 8) S. Geller and M. A. Gilleo, J. Phys. Chem. Solids **3**, 30 (1957).
- 9) R. Pauthenet, Ann. Phys. **13**, 424 (1958).
- 10) S. Geller, H. J. Williams, R. C. Sherwood, J. P. Remeika, and G. P. Espinosa, Phys. Rev. **131**, 1080 (1963).
- 11) S. Geller, J. P. Remeika, R. C. Sherwood, H. J. Williams, and G. P. Espinosa, Phys. Rev. **137**, A1034 (1965).
- 12) J. T. Chang, J. F. Dillon, and U. F. Gianola, J. Appl. Phys. **36**, 1110 (1965).
- 13) K. Chow, W. Leonard, and R. Comstock, IEEE Trans. Mag. **4**, 416 (1968).
- 14) T. Nelson, IEEE Trans. Mag. **4**, 421 (1968).
- 15) J. S. van Wieringen, Phys. Rev. **90**, 488 (1953).
- 16) T. R. McGuire, Phys. Rev. **97**, 831 (1955).
- 17) J. Kaplan and C. Kittel, J. Chem. Phys. **21**, 760 (1953).
- 18) R. K. Wangsness, Phys. Rev. **91**, 1085 (1953).
- 19) R. K. Wangsness, Phys. Rev. **93**, 68 (1954).
- 20) N. Tsuya, Prog Theor Phys **12**, 1 (1954).
- 21) R. K. Wangsness, Phys. Rev. **97**, 831 (1955).
- 22) S. Geschwind and L. R. Walker, J. Appl. Phys. **30**, S163 (1959).
- 23) J. H. Van Vleck, Phys. Rev. **123**, 58 (1961).
- 24) M. Imai, Y. Ogata, H. Chudo, M. Ono, K. Harii, M. Matsuo, Y. Ohnuma, S. Maekawa, and E. Saitoh, Appl. Phys. Lett. **113**, 052402 (2018).
- 25) M. Imai, H. Chudo, M. Ono, K. Harii, M. Matsuo, Y. Ohnuma, S. Maekawa, and E. Saitoh, Appl. Phys. Lett. **114**, 162402 (2019).
- 26) M. Imai, H. Chudo, M. Matsuo, S. Maekawa, and E. Saitoh, Phys. Rev. B **102**, 014407 (2020).
- 27) S. J. Barnett, Phys. Rev. **6**, 239 (1915).
- 28) X. Jiang, L. Gao, J. Z. Sun, and S. S. P. Parkin, Phys. Rev. Lett. **97**, 217202 (2006).
- 29) C. D. Stanciu, A. Tsukamoto, A. V. Kimel, F. Hansteen, A. Kirilyuk, A. Itoh, and Th. Rasing, Physical Review Letters **99**, 217204 (2007).
- 30) K.-J. Kim, S. K. Kim, Y. Hirata, S.-H. Oh, T. Tono, D.-H. Kim, T. Okuno, W. S. Ham, S. Kim, G. Go, Y. Tserkovnyak, A. Tsukamoto, T. Moriyama,

- K.-J. Lee, and T. Ono, Nat. Mater. **16**, 1187 (2017).
- 31) S. K. Kim, K. Nakata, D. Loss, and Y. Tserkovnyak, Phys. Rev. Lett. **122**, 057204 (2019).
- 32) T. Moriya, Prog. Theor. Phys. **16**, 23 (1956).
- 33) A. H. Mitchell, J. Chem. Phys. **27** 17 (1957).
- 34) D. Beeman and P. Pincus, Phys. Rev. **166**, 359 (1968).
- 35) S. V. Tyablikov, Ukrain. Math. Zh. **11**, 287 (1959).
- 36) T. Oguchi and A. Honma, J. Appl. Phys., **34**, 1153 (1963).
- 37) M. Mori, J. Phys. Soc. Jpn. **86**, 124705 (2017).
- 38) J. H. van Vleck, in *The Theory of Electric and Magnetic Susceptibilities* (Oxford University Press, New York, 1932).
- 39) P. G. de Gennes, Comptes Rendus **247**, 1836 (1958).
- 40) A. Szutula, and J. Leciejewicz, in *Handbook on the Physics and Chemistry of Rare Earths* vol. 12, eds. K. A. Gschneider, Jr. and L. Eyring (Elsevier, Amsterdam, 1989) p. 131.
- 41) J. S. Plant, Journal of Physics C: Solid State Physics **10**, 4805 (1977).
- 42) Y. Nambu, J. Barker, Y. Okino, T. Kikkawa, Y. Shiomi, M. Enderle, T. Weber, B. Winn, M. Graves-Brook, J.M. Tranquada, T. Ziman, M. Fujita, G.E.W. Bauer, E. Saitoh, K. Kakurai, Phys. Rev. Lett. **125**, 027201 (2020).